Continuum Mech. Thermodyn. (2009) 21: 17–26
DOI 10.1007/s00161-009-0096-2

ORIGINAL ARTICLE

F. J. Pérez-Reche · L. Truskinovsky · G. Zanzotto

Martensitic transformations: from continuum mechanics to spin models and automata

Received: 4 February 2009 / Accepted: 4 February 2009 / Published online: 17 March 2009

Abstract We present a new procedure for the systematic reduction of a continuum theory of martensitic transformations to a spin system whose dynamics can be described by an automaton. Our prototypical model reproduces most of the experimental observations in martensites associated with criticality and power-law acoustic emission. In particular, it explains in a natural way why cyclic training is necessary to reach scale-free behavior.

Keywords Avalanches · Criticality · Spin models · Automata

PACS 62.20.F-, 64.60.My, 81.30.Kf, 89.75.Fb

1 Introduction

Both acoustic and calorimetric by signals which are routinely detected in shape-memory alloys submitted to quasi-static loading have a marked by intermittent character [1–4]. Such behavior indicates that the finite strain effect associated with the martensitic transformation in a steadily driven system splits into a set of strain avalanches of different sizes which reflect transitions between neighboring metastable states [1–5]. A statistical analysis shows that after multiple thermal cycling through the transition the amplitudes of the avalanches evolve towards a power-law distribution [2,3]. This means that during such a loading and reloading process (training), shape-memory alloys self organize towards criticality. In this sense martensites[1] are essentially different from many other apparently similar systems, say driven ferromagnets displaying Barkhausen noise, because in those systems training is not required to reach a scale-free behavior.

Criticality has attracted a great deal of interest over the last decades due to its ubiquity in nature, as power-law distributions have been reported in a wide variety of complex systems [7,8]. At criticality there are no characteristic length scales and microscopic details do not play a crucial role. This generates classes of

[1] Except those with very small spontaneous strain [6].

Communicated by S. Seelecke

F. J. Pérez-Reche
Department of Chemistry, University of Cambridge, Cambridge CB2 1EW, UK

L. Truskinovsky (✉)
Laboratoire de Mécanique des Solides, CNRS UMR-7649, Ecole Polytechnique,
Route de Saclay, 91128 Palaiseau, France
E-mail: trusk@lms.polytechnique.fr

G. Zanzotto
Dipartimento di Metodi e Modelli Matematici per le Scienze Applicate, Università di Padova,
Via Trieste 63, 35121 Padua, Italy

universal behavior which can be studied by means of relatively simple, prototypical models. Thus, sandpile automata, showing self-organized criticality (SOC) [9], and driven models of the Ising type with quenched disorder, showing classical criticality [10], are known to give different prototypes, which are expected to represent broad classes of avalanche-mediated behaviors observed in physical systems as diverse as magnetics and earthquakes.

Within the context of martensites, considerable recent effort has also been devoted to understanding the mechanisms leading to criticality. A qualitative link to SOC has been established early on in [1,11]. Quantitative models implying the existence of continuous disorder-induced phase transitions as in spin systems with quenched disorder have been studied by many groups (see for instance [12]). Large scale numerical simulations of cyclically loaded martensites within the framework of classical elasticity have been performed in [13,14]. Finally, there has been a recent attempt to link martensites to spin glasses [15]. While a scale-free behavior is predicted by some of the above approaches, none of these can in principle explain why criticality in martensites requires cycling and why the power-law acoustic emission is observed only after a plasticity-like shakedown.

In a recent paper [16] we proposed an explanation for the emergence of criticality in martensites based on the experimental evidence of considerable dislocational activity in cyclically-driven shape-memory alloys [17–21]. In this paper we conjecture that the disorder needed for criticality in martensites is not quenched but is acquired by the system in the process of training. Here we provide additional details on the methods leading to this conclusion, which are based on the reduction of a continuum elasticity theory first to a discrete spin model and then to an automaton of a sand-pile type. The resulting prototypical system preserves all the essential features of the original continuum model, and it captures all the three major phenomena: phase transformation, twinning, and plasticity. Most importantly, the model accounts for training-induced criticality in martensites, including the prediction of such fine features of the scale-free nonequilibrium steady state as the shape of avalanches and the complex nature of the emerging spatial disorder.

2 Model

2.1 Tensorial formulation

We start with a classical continuum theory of martensites which is based on the assumption that the elastic energy density is a nonconvex function of the deformation gradient, e.g. [22,23]. The general structure of this function in 2D has been characterized in [24,25].

The first step of our reduction procedure is a spatial discretization of the continuum model allowing one to represent a 2D Bravais lattice as a collection of N kinematically compatible units. For each unit i we define the basis vectors $\{\mathbf{u}_1^i, \mathbf{u}_2^i\}$. The energy of the whole body at temperature θ is given by

$$\Phi = \Phi_1(\{\mathbf{u}_a^i\}; \theta) + \Phi_2(\{\mathbf{u}_a^i, \mathbf{u}_a^j\}; \theta), \tag{1}$$

where Φ_1 is the energy of the noninteracting elastic units and Φ_2 is the interaction energy which is taken to be quadratic. We assume that

$$\Phi_1 = \sum_{i=1}^{N} \phi(\mathbf{u}_a^i; \theta), \tag{2}$$

where ϕ is the energy of a unit. From the fact that ϕ defines the response of a homogeneous Bravais lattice, we deduce the following two invariance properties [22]:

(i) It must be invariant under rigid rotations $\mathbf{Q}$ of the lattice. As a consequence, it does not depend on individual lattice vectors but on the lattice-metric $\mathbf{C}$ with elements $C_{ab} = \mathbf{u}_a \cdot \mathbf{u}_b$.

(ii) It must be invariant under the change of bases generating the same lattice. Two bases $\{\mathbf{u}_a\}$ and $\{\mathbf{v}_a\}$ describe the same lattice if and only if $\mathbf{v}_a = \sum_{b=1}^{2} m_a^b \mathbf{u}_b$, where m_a^b are the elements of matrices $\mathbf{M}$ in $GL(2, \mathbb{Z})$.[2] The function ϕ then satisfies $\phi(\mathbf{C}; \theta) = \phi(\mathbf{M}^t \mathbf{C} \mathbf{M}; \theta)$.

In 2D the five possible Bravais lattices can be represented in the 'fundamental domain' which is located in the lattice-metrics space (FD, Fig. 1). The austenite (high θ) and martensite (low θ) phases correspond to wells

[2] $GL(2, \mathbb{Z})$ is the group of 2×2 invertible matrices with integral entries.

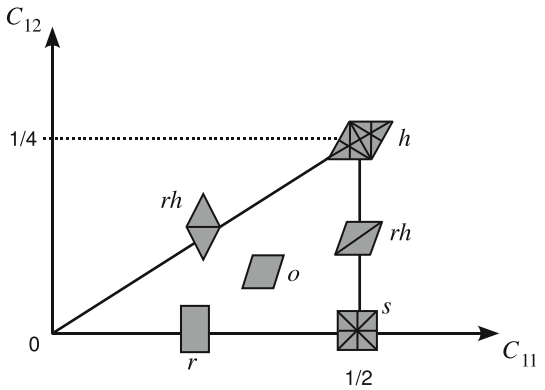

Fig. 1 Projection on the plane (C_{11}, C_{12}) of the intersection of the fundamental domain (FD) with the plane $C_{11} + C_{22} = 1$. The location in FD of each of the Bravais types (*o* oblique, *r* rectangular, *rh* rhombic, *s* square, *h* hexagonal) is schematically shown

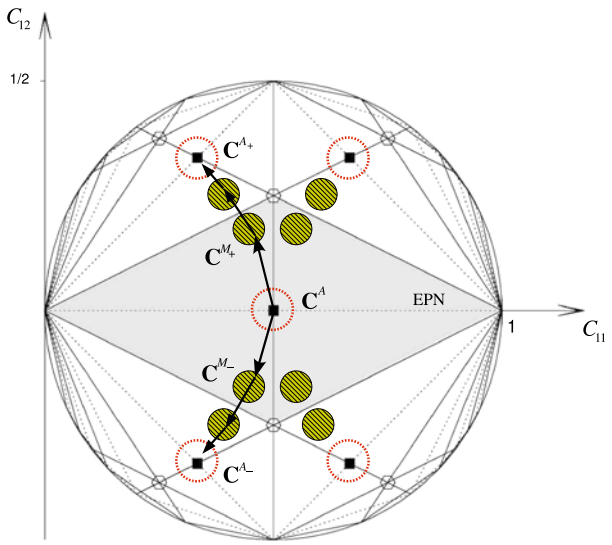

Fig. 2 Section on the plane $C_{11} + C_{22} = 1$ of the space of 2D lattice metrics. The infinitely many $GL(2, \mathbb{Z})$-related replicas of the fundamental domain shown in Fig. 1 fill the whole space of metrics. The *shaded area* is the maximal EPN for the square structure $\mathbf{C}^A$. *Empty and hatched circles* indicate austenite $\mathbf{M}^t\mathbf{C}^A\mathbf{M}$ and martensite $\mathbf{M}^t\mathbf{C}^M\mathbf{M}$ energy wells, respectively. The *arrows* show the particular transformation path considered in the text (Color figure online)

of $\phi(\mathbf{C}; \theta)$ in FD at $\mathbf{C}^A$ and $\mathbf{C}^M$, respectively. Owing to the $GL(2, \mathbb{Z})$-invariance, the energy $\phi(\mathbf{C}; \theta)$ has infinitely many symmetry-related copies of such wells located at $\mathbf{M}^t\mathbf{C}^A\mathbf{M}$ and $\mathbf{M}^t\mathbf{C}^M\mathbf{M}$, where $\mathbf{M} \in GL(2, \mathbb{Z})$. Figure 2 shows some of the $GL(2, \mathbb{Z})$-related replicas of FD and the energy wells corresponding to a transition from square austenite to oblique martensite (see [25] for more details).

2.2 Periodic energy landscape

We note that the classical description of martensitic transformations based solely on Landau theory may be viewed as particular cases of the general framework described above. The Landau theory considers energy wells only inside the Ericksen–Pitteri Neighborhood (EPN) of the austenite phase. The EPN is defined as a subset in the space of metrics in which the global $GL(2, \mathbb{Z})$-invariance reduces to the invariance under the austenite point group. It contains one autenite well and a finite number of martensite wells corresponding to different martensitic variants. For instance, the EPN corresponding to the square austenite contains four oblique variants of martensite (Fig. 2). Such a description is expected to be sufficient when the transformation distortion is small and the energy barriers for slip are much higher than the barriers for phase transformation and twinning.

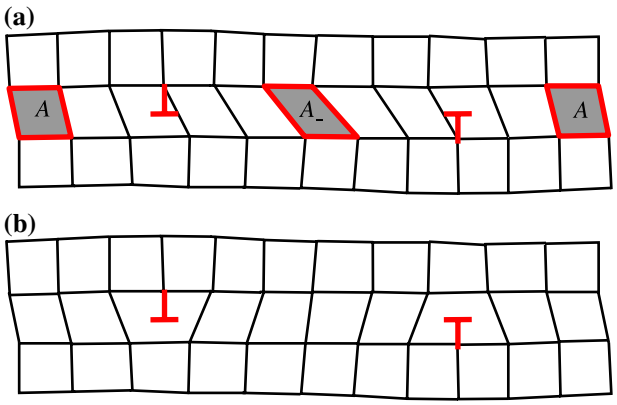

Fig. 3 Two representations of a 2D dislocation loop. **a** Continuous lattice deformation in terms of kinematically compatible units as considered in the text. The *shaded units* correspond to the austenite structure A in the EPN and the replica A_- outside the EPN introducing the dislocation loop. **b** Classical interpretation involving discontinuous deformations with nonzero Burgers vectors (Color figure online)

The general theory considered here takes into account large distortions outside the EPN which are responsible for the formation of dislocations [24,25]. Therefore the interplay between the phase transformation and the creation and evolution of such defects can be studied in a natural way within the present framework. We emphasize that the continuity of displacements does not prevent dislocations from nucleating or propagating as is exemplified in Fig. 3 where we compare the continuous representation of the displacement field assumed in this work (see Fig. 3a) with the standard representation containing discontinuities (see Fig. 3b). The deformation field in Fig. 3 corresponds to two dislocations with opposite sign forming a dislocation loop. We mention that a version of the Landau theory with discontinuous displacements which assumes a conventional description of dislocations as in Fig. 3b has been recently proposed in [26].

To analyze the main consequences of the global periodicity of the energy density, we introduce a specific transformation path from square to oblique as indicated by the arrows in Fig. 2. In spite of its simplicity, this path captures the main ingredients of the energy landscape, namely, the multi-variant nature of the martensitic phase (which generates twinning) and the presence of infinitely many copies of the EPN (allowing for slip). In 2D the deformation along the transformation path $\mathbf{C}(t)$ can be written in terms of three scalar order parameters $e(\mathbf{C}(t))$, $e'(\mathbf{C}(t))$, and $e''(\mathbf{C}(t))$. The non-convexity of ϕ associated with the phase transformation, twinning and slip will be fully carried by its nonconvex dependence on the primary order parameter $e(\mathbf{C})$; in contrast, we assume that ϕ is a convex (quadratic) function of the non-order parameters $e'(\mathbf{C})$ and $e''(\mathbf{C})$.

2.3 Scalar formulation

The relaxation of the harmonic variables $e'(\mathbf{C})$ and $e''(\mathbf{C})$ can be assumed as instantaneous (in the time scales of both driving and relaxation of the primary order parameter), so they can be adiabatically eliminated. By using the corresponding linear equilibrium equations together with the kinematic compatibility constraints we can rewrite the elastic energy Eq. (1) in terms of the scalar variables e_i only

$$\widetilde{\Phi}(e;\theta) = \sum_{i=1}^{N} f(e_i;\theta) + \frac{1}{2}\sum_{i,j=1}^{N} K_{ij} e_i e_j, \tag{3}$$

where $\mathbf{K} = \{K_{ij}\}$ is the kernel describing the elastic interactions between different units and incorporating both the original interaction energy Φ_2 and the additional nonlocal interactions due to the compatibility constraints [27]. The renormalized energy of an elastic unit, $f(e;\theta)$, inherits the properties of $\phi(\mathbf{C};\theta)$ including the $GL(2,\mathbb{Z})$-invariance. We approximate f by a periodic function with three-parabolic form in each period, where each of the three parabolas is given by the same expression, $f(e;\theta) = \frac{1}{2}(e-w)^2 + g(\theta)s^2$, with different parameters w and s (see Fig. 4). The parameter $w = d + \bar{e}s$ defines the location of the bottoms of the energy wells in terms of the two discrete variables: $s = 0, \pm 1$ and $d \in \mathbb{Z}$; $\bar{e}$ is the transformation strain. The parameter s accounts for the phase transition: $s = 0$ in the austenite, and $s = \pm 1$ in the two variants

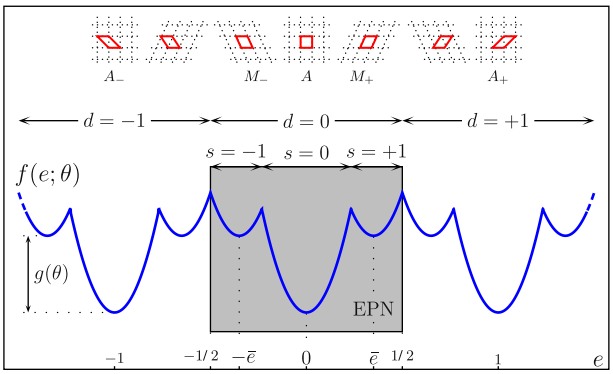

Fig. 4 Representation of the on-site periodic potential $f(e;\theta)$. The quantities $s, d, g(\theta)$, and $\bar{e}$ characterizing $f(e;\theta)$ are explicitly indicated. The *shaded box* highlights the EPN. Configurations show the lattice structures corresponding to the bottoms of the potential wells, with lattice cells marked for the austenite A and for the two variants of martensite $M_\pm$ in the EPN. Configurations $A_\pm$ are the first two replicas of A outside the EPN (Color figure online)

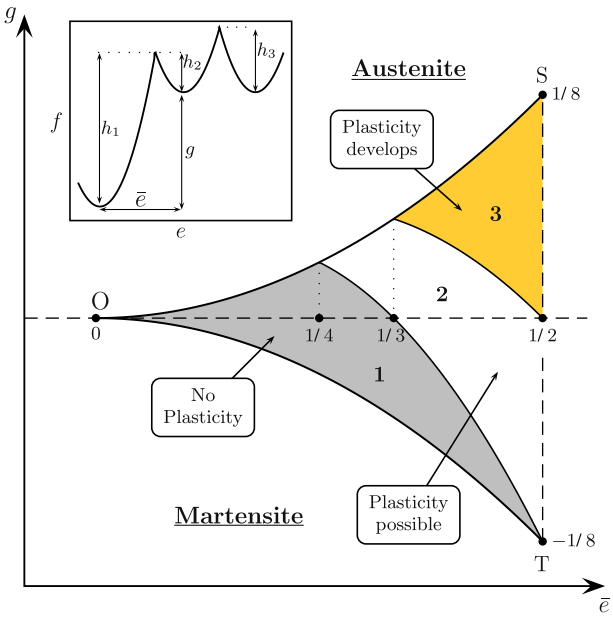

Fig. 5 Phase diagram for a homogeneous system in the space $(\bar{e}, g)$. The *inset* indicates the energy barriers h_1, h_2, h_3 used to define three characteristic zones in the domain of phase coexistence *SOT*, as explained in the text (Color figure online)

of martensite. The value of d specifies the period of f. Finally, the function $g(\theta)$ measures the difference in energy between austenite the and martensite. We implement thermal driving by changing periodically the preference between austenite and martensite through cycling $g(\theta)$ at constant rate.

To understand the role of the parameters g and $\bar{e}$ in the model, it is instructive to consider the $(\bar{e}, g)$ phase diagram for a homogeneous system (i.e., with $\mathbf{K} = \mathbf{0}$) shown in Fig. 5. The stability boundaries for the martensite and the austenite phases are indicated by the lines *OS* and *OT*, respectively. The limit $\bar{e} \to 0$ gives a fully reversible transformation, while $\bar{e} = 1/2$ corresponds to a reconstructive transformation. The possible behaviors for intermediate $\bar{e}$ can be heuristically classified into three classes corresponding to the three zones indicated in Fig. 5. In zone **1** the activation energy necessary to escape from the austenite well, h_1, is smaller than the barrier between the martensite well and the next EPN, h_3. Slip may then be typically excluded. In contrast, the martensitic transformation may naturally lead to slip in zones **2** and **3** where h_3 is smaller than h_1. This will surely be the case for systems in zone **3** where the barrier for the reverse martensitic transformation, h_2, is smaller than h_3. Shape-memory alloys exhibiting a pronounced shakedown behavior such as CuZnAl and NiTi have an almost reconstructive transformation strain [28], and can be confidently placed in zone **3**.

2.4 Continuous dynamics

The martensitic transformation has a markedly athermal character [29] at least for the shape-memory alloys we are interested in, and we can consider a purely mechanical setting. We assume that the continuous dynamics is overdamped and write the dimensionless evolution equation for the field $\mathbf{e} = \{e_i\}$ in the form

$$\frac{\partial \mathbf{e}}{\partial t} = -\gamma \frac{\partial \widetilde{\Phi}(\mathbf{e};\theta)}{\partial \mathbf{e}}, \tag{4}$$

where γ is the ratio of the rate of relaxation to the rate of driving. In the quasi-static limit (i.e., $\gamma \to \infty$), the dynamics projects on the local minima of $\widetilde{\Phi}$ which form a discrete set of branches. The system remains on a particular equilibrium branch until it becomes unstable due to the driving. For smooth energies $\widetilde{\Phi}$, the marginally stable configurations correspond to points where the Hessian of $\widetilde{\Phi}$ becomes degenerate (i.e., $\det \|\partial^2 \widetilde{\Phi}/\partial \mathbf{e}^2\| = 0$), which is in general a global condition [5,30].

In the case of the piece-wise quadratic energy $f(e;\theta)$, the equilibrium equations $\partial \widetilde{\Phi}/\partial \mathbf{e} = \mathbf{0}$ give

$$\mathbf{e}(\mathbf{s},\mathbf{d}) = (\mathbf{I}+\mathbf{K})^{-1}(\mathbf{d}+\bar{e}\mathbf{s}), \tag{5}$$

where $\mathbf{I}$ is the identity matrix, $\mathbf{s} = \{s_i\}$, and $\mathbf{d} = \{d_i\}$. This allows us to adiabatically eliminate the remaining continuous degrees of freedom which are in this case harmonic. The stability conditions become local and can be explicitly written as $e^-(s_i,d_i;g) < e_i < e^+(s_i,d_i;g)$ for every unit i, where

$$e^{\pm}(s_i,d_i;g) = \begin{cases} w_i \pm (\bar{e}/2 + g/\bar{e}), & s_i = 0, \\ w_i \pm (\bar{e}/2 - g/\bar{e}), & s_i = \mp 1, \\ w_i \pm (1-2\bar{e})/2, & s_i = \pm 1. \end{cases} \tag{6}$$

The first two cases correspond to the direct and to the reverse martensitic transformation, respectively. The third limit corresponds to the creation of a slip. When the stability condition is violated by at least one unit, the resulting instability resolves through an avalanche which brings the system to another equilibrium branch characterized by different values of $\mathbf{s}$ and $\mathbf{d}$. Since these variables are discrete, the continuous dynamics (4) gives rise to a series of jumps [5].

2.5 Spin model

By eliminating the continuous variables from Eq. (3), we can rewrite the relaxed energy in terms of the variables $\mathbf{s}$ and $\mathbf{d}$. The resulting Hamiltonian is of the *Potts* type:

$$\widehat{\Phi} = -\sum_{i,j}\left[\frac{\bar{e}^2}{2}\left(J_{ij} - \frac{2g}{\bar{e}^2}\delta_{ij}\right)s_i s_j + \frac{1}{2}J_{ij}d_i d_j + \bar{e}J_{ij}s_i d_j\right], \tag{7}$$

where $\mathbf{J} = (\mathbf{I}+\mathbf{K})^{-1} - \mathbf{I}$ is the matrix of effective interaction. Here the spin variable $\mathbf{s}$, describing the martensitic phase transition and twinning, is analogous to similar variables in the conventional spin models of martensitic phase transitions [12,15]. The new integer-valued variable $\mathbf{d}$ describes the slip. It has the same meaning as the lattice incompatibility measures introduced in classical models of plasticity employing discontinuous displacements (e.g. [26]). Because $\mathbf{d}$ follows a threshold dynamics, this variable cannot be adiabatically eliminated and the resulting problem cannot be easily formulated in terms of $\mathbf{s}$ only.

Instead of deriving the expression for $\mathbf{J}$ from its explicit representation above through $\mathbf{K}$, we follow the approach of [16] and postulate directly the structure of the kernel capturing the main expected features: anisotropy and sign indefiniteness [31]. More specifically, we assume $\mathbf{J}$ to be of the ANNNI type:

$$J_{ij} = \begin{cases} J_0, & i = j, \\ J_1 > 0, & i \text{ n.n. } j, \\ -J_2 < 0, & i \text{ n.n.n. } j, \\ 0, & \text{otherwise}, \end{cases} \tag{8}$$

where 'n.n.' and 'n.n.n.' indicate nearest and next-to-nearest neighbors, respectively. This simple hypothesis accounts for the competing interactions driving the coarsening and the refinement of the microstructure [32,33]. In order to penalize the inhomogeneity of the field $\mathbf{w}$ the self-interaction term is chosen to satisfy $J_0 = J_{ii} = -\sum_{i\neq j} J_{ij}$. Our unpublished work shows that these assumptions on $\mathbf{J}$ reflect rather faithfully the structure of the matrix obtained from a lattice model with an interaction $\mathbf{K}$ derived from kinematic compatibility. For instance, despite the short-range structure of the renormalized $\mathbf{J}$, the background kernel $\mathbf{K} = (\mathbf{I}+\mathbf{J})^{-1} - \mathbf{I}$ describing elastic interactions in our prototypical lattice has a long-range character.

2.6 Automaton

The jump process described above can be conveniently represented as a *sandpile automaton*. To this end we assume that the elastic strain $\delta_i = e_i - w_i$ represents the 'local height' of the sand-pile. From Eq. (6) and the definition of $\mathbf{J}$, we obtain that $\delta_i = \sum_j J_{ij}(s_j + \bar{e}d_j)$. The dependence on temperature is fully contained in the variables $\delta^{\pm}(s_i; g(\theta)) = e^{\pm}(s_i, d_i; g) - w_i$ which enter the stability condition $\delta^-(s_i, g) < \delta_i < \delta^+(s_i, g)$. In contrast to $e^{\pm}$ (Eq. 6), the limits of stability $\delta^{\pm}$ do not depend on $\mathbf{d}$ (i.e., they are independent of the EPN).

Once a cell i becomes unstable (i.e., the condition $\delta^- < \delta_i < \delta^+$ is violated), the strain variable passes to a neighboring energy well. As a consequence, the location of the bottom of the well w_i updates to $w_i + r$, where $r = \pm\bar{e}$ for phase transitions ($s_i = 0 \leftrightarrow s_i = \pm 1$) and $r = \pm(1 - 2\bar{e})$ for slips ($s_i = \pm 1 \rightarrow s_i = \mp 1$, $d_i \rightarrow d_i \pm 1$). Such rearrangement produces an update in $\boldsymbol{\delta}$,

$$\delta_j \rightarrow \delta_j + J_{ij} r, \tag{9}$$

which, given our assumptions concerning (8), can be rewritten in the form

$$\begin{aligned} \delta_i &\rightarrow \delta_i - 4(J_1 - J_2)r \\ \delta_j &\rightarrow \delta_j + J_1 r, \quad j \text{ nearest neighbors of } i, \\ \delta_k &\rightarrow \delta_k - J_2 r, \quad k \text{ next-to-nearest neighbors of } i. \end{aligned} \tag{10}$$

Notice that each update may make new sites unstable, and therefore the updates must continue at constant g until the system is fully equilibrated. The total number of updates before stabilization defines the size A of an avalanche. We assume open boundary conditions so that the update of the total elastic strain $\Delta = \sum_j \delta_j$ (when the cell i becomes unstable) is

$$\Delta \rightarrow \Delta - \begin{cases} 0, & i \in \text{bulk}, \\ (J_1 - 2J_2)r, & i \in \text{edge}, \\ (2J_1 - 3J_2)r, & i \in \text{corner}. \end{cases} \tag{11}$$

The automaton variable is then conserved for all the updates except those originated at the boundaries of the system. The inequality[3] $J_1 > 2J_2$ guarantees that during the avalanches the stress is released (at a rate which decreases with N as $N^{-1/3}$). This 'dissipation' mechanism together with the quasi-static driving provide the necessary conditions for the system to reach a self-organized stationary state [34].

3 Numerical results

The automaton introduced in the previous section can be easily implemented numerically. Here we present the numerical results corresponding to an almost reconstructive transformation with $\bar{e} = 0.47$ inside zone **3** in Fig. 5. We work on a square grid with 501×501 units and assume that $J_1 = 0.062$ and $J_2 = 0.03$ which ensure that the dissipation inequality is satisfied. We impose a synchronous dynamics such that all the unstable cells are updated simultaneously as the discrete time increases by one unit. The number of simultaneous updates in an avalanche defines its duration T. The initially homogeneous austenite is arbitrarily chosen to contain four dislocation loops (see one of them in Fig. 3) placed at randomly chosen locations; assuming only one initial loop gives similar results [16].

[3] In the language of sandpile automata, the condition $J_1 > 2J_2$ ensures that grains of sand are lost at the boundaries of the system.

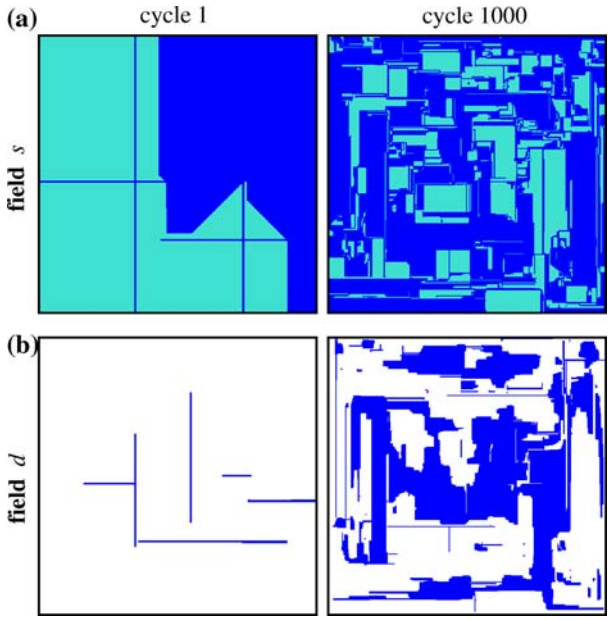

Fig. 6 Evolution of the phase and defect microstructures in the lattice during thermal cycling. Four dislocation loops are initially placed in random locations. **a** Configuration of the martensitic phase domains, represented by the field s_i, after cycle 1 and cycle 1000 (*light and dark* indicate $s = 1$ and $s = -1$, respectively). **b** The corresponding configurations of the slip variable d. *White and dark* colors indicate $d = 0$ and $d \neq 0$ (mostly $|d| = 1$), respectively (Color figure online)

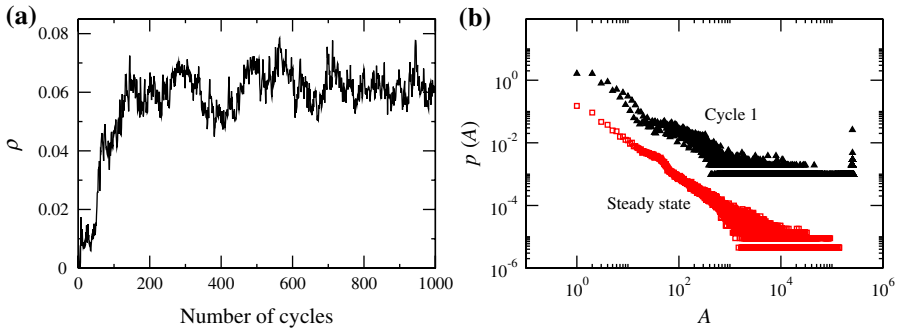

Fig. 7 Evolution towards a critical steady state. **a** Dislocation density ρ during the first 1,000 cycles. **b** Distribution of the avalanche sizes after cycle 1 (*triangles*) and in the stationary-state after 1,000 cycles (*squares*). The distribution for the first cycle (displaced vertically for clarity) has been obtained by averaging over 800 realizations of the system with different location of the initial dislocations. The distribution in the stationary state has been obtained by averaging over the last 800 cycles in the series with 1,000 transformations (Color figure online)

Figure 6a shows the spatial distribution of **s** in the martensitic phase after cycle 1 and after cycle 1000. The complexity of the phase microstructure clearly increases during the training period. The system develops a certain amount of plastic deformation ($d \neq 0$) induced by the phase transition as shown in Fig. 6b. We monitor the level of plastic deformation through the density ρ of nearest neighbors with differing values of d_i (our measure of dislocation density). As shown in Fig. 7a, the evolution of ρ is marked by a steep initial increase (training period) which after approximately 150 cycles leads to a steady regime (shakedown).

To compare our model with experiments where the acoustic emission during the transformation was detected, we link the size of the avalanches in the model with the acoustic bursts in experiments. As shown in Fig. 7b, the distribution of avalanche sizes $p(A)$ evolves from a supercritical behavior (peak at large values of A) during the first cycles towards a power law in the steady-state regime.

We observe that in the present framework, the scale-free size distribution does not necessarily imply scale-free distribution of durations, $p(T)$, as shown in Fig. 8a. This is a consequence of our simplifying assumptions; the model starts to generate a power-law structure of durations as soon as a small amount of quenched disorder is introduced (in the form of a Gaussian distribution of the initial δ_i with zero mean and standard deviation r).

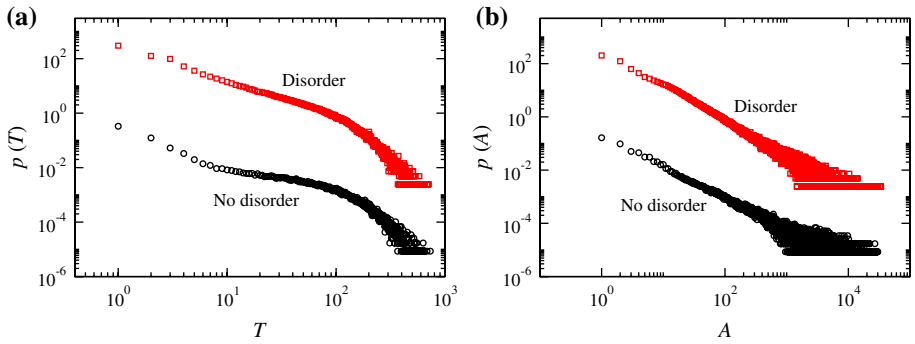

Fig. 8 Distributions of avalanche **a** durations and **b** sizes in the steady state attained after 1,000 cycles with initial quenched disorder ($r = 0.01$) and without ($r = 0$)

When the initial disorder is small such modification does not influence significantly the power-law character of $p(A)$ (Fig. 8b); big amounts of disorder prevent large avalanches from occurring and the probability distributions develops a subcritical cut-off [10].

Besides the power-law statistics and the microstructure complexity, the proposed model accounts for other experimental observations in martensites such as hysteresis shakedown and asymmetric signal shapes (see [16] for more detail).

4 Conclusions

Our main conclusion is that SOC originates in martensites from the interplay between the reversible phase change and the irreversible development of an optimal amount of plastic deformation. We emphasize that the disorder responsible for criticality is not imposed through initial inhomogeneity but is created by the system itself. This suggests that the emergence of scale-free behavior in the proposed model is an example of a jamming transition.

The phase transition in our picture occurs through intermittent dynamics with large fluctuations which lead to permanent changes in the system. Most of these changes take place during the training period. This period is finite because the dislocational activity eventually saturates: despite periodicity of the 'homogeneous' energy landscape the convex interaction term in the energy makes successive slips progressively more and more expensive.

One of the most unexpected outcomes of the model is that the whole wealth of phenomena accompanying self-organization to criticality in martensites can be captured, at least qualitatively, in a relatively simple 2D spin model with a standard threshold dynamics. The main advantage of this minimal model comparing to its more detailed analogs, say [13,14,26], is its full mathematical transparency allowing one to pursue the origin of scale-free behavior analytically. It comes at a cost because due to the schematic treatment of the long-range interactions, of the inertial dynamics, and of the relative energetic cost of twin and phase interfaces, the model does not capture the process of self-organization in full quantitative detail. Among the omitted effects we particularly mention the elastic incompatibility of the energy wells which is known to be important for the level of reversibility achieved by a martensitic transformation [35]. In order to ensure an engineering level of agreement of the theory with experiments, more realistic models of the computational nature must be pursued in parallel to the prototypical treatment presented here.

We mention that while we have limited ourselves in this paper to temperature-driven martensitic transformations, our theoretical framework offers a tool for studying self-organization in systems subjected to mechanical driving as well. An example of such a study, exploring the effect of the stiffness of the loading device on the critical exponents, and investigating the possibility of driving-induced crossover between different universality classes, can be found in [36].

Acknowledgments We acknowledge partial funding from EU contract MRTN-CT-2004-505226.

References

1. Vives, E. et al.: Distribution of avalanches in martensitic transformations. Phys. Rev. Lett. **72**, 1694 (1994)
2. Carrillo, L. et al.: Experimental evidence for universality of acoustic emission avalanche distributions during structural transitions. Phys. Rev. Lett. **81**, 1889 (1998)
3. Pérez-Reche, F.J. et al.: Kinetics of martensitic transitions in Cu-Al-Mn under thermal cycling: Analysis at multiple length scales. Phys. Rev. B **69**, 064101 (2004)
4. Pérez-Reche, F.J. et al.: Driving rate effects in avalanche-mediated first-order phase transitions. Phys. Rev. Lett. **93**, 195701 (2004)
5. Puglisi, G., Truskinovsky, L.: Thermodynamics of rate independent plasticity. J. Mech. Phys. Solids **53**, 655–679 (2005)
6. Pérez-Reche F.J., Vives E., Mañosa L., Planes A.: Calorimetric and acoustic emission study of the premartenstic and martensitic transitions in Ni–Mn–Ga. Mater. Sci. Eng. A **378**, 353–356 (2004)
7. Sornette, D.: Critical Phenomena in Natural Sciences. Springer, Berlin (2000)
8. Newman, M.E.J.: Power laws, Pareto distributions and Zipf's law. Contemp. Phys. **46**, 323–351 (2004)
9. Bak, P.: How nature works: the science of self-organized criticality. Oxford University Press, Oxford (1997)
10. Sethna, J.P., Dahmen, K.A., Perković, O. : Random-field Ising models of hysteresis. In: Bertotti, G., Mayergoyz, I.D. (eds.) The Science of Hysteresis II, Academic Press, New York (2006)
11. Goicoechea, J., Ortín, J.: Hysteresis and return-point memory in deterministic cellular automata. Phys. Rev. Lett. **72**, 2203 (1994)
12. Cerruti, B., Vives, E.: Random-field potts model with dipolarlike interactions: Hysteresis, avalanches, and microstructure. Phys. Rev. B **77**, 064114 (2008)
13. Sreekala, S., Ahluwalia, R., Ananthakrishna, G.: Precursors and power-law statistics of acoustic emission and shape memory effect in martensites. Phys. Rev. B **70**, 224105 (2004)
14. Salman, O.U., Finel, A.: Avalanches in fluctuationless martensitic transitions. In: The International Conference On Martensitic Transformations, Santa Fe, July (2008)
15. Sherrington, D.: A simple spin glass perspective on martensitic shape-memory alloys. J. Phys. Condens. Matter **20**, 304213 (2008)
16. Pérez-Reche, F.J., Truskinovsky, L., Zanzotto, G.: Training-induced criticality in martensites. Phys. Rev. Lett. **99**, 075501 (2007)
17. Ríos-Jara, D., Guénin, G.: On the characterization and origin of the dislocations associated with the two way memory effect in Cu-Zn-Al thermoelastic alloys–I. Qualitative analysis of the dislocations. Acta Metall. **35**, 109–119 (1987)
18. Pons, J., Lovey, F.C., Cesari, E.: Electron microscopy study of dislocations associated with thermal cycling in a Cu-Zn-Al shape memory alloy. Acta Metall. Mater. **38**, 2733–2740 (1990)
19. Lovey, F.C., Torra, V.: Shape memory in Cu-based alloys: phenomenological behavior at the mesoscale level and interaction of martensitic transformation with structural defects in Cu-Zn-Al. Prog. Mater. Sci. **44**, 189–289 (1999)
20. Miyazaki, S., Ishida, A.: Martensitic transformation and shape memory behavior in sputter-deposited TiNi-base thin films. Mater. Sci. Eng. A **273–275**, 106–133 (1999)
21. Cuniberti, A., Romero, R.: Differential scanning calorimetry study of deformed CuZnAl martensite. Scr. Mater. **51**, 315–320 (2004)
22. Ericksen, J.L.: Some phase transitions in crystals. Arch. Ration. Mech. Anal. **73**, 99–124 (1980)
23. Tolédano, P., Dmitriev, V.: Reconstructive Phase Transitions. World Scientific, Singapore (1996)
24. Bhattacharya, K. et al.: Crystal symmetry and the reversibility of martensitic transformations. Nature **428**, 55–59 (2004)
25. Conti, S., Zanzotto, G.: A variational model for reconstructive phase transformations in crystals, and their relation to dislocations and plasticity. Arch. Ration. Mech. Anal. **173**, 69–88 (2004)
26. Gröger, R., Lookman, T., Saxena, A.: Defect-induced incompatibility of elastic strains: dislocations within the Landau theory of martensitic phase transformations. Phys. Rev. B **78**, 184101 (2008)
27. Lookman, T. et al.: Ferroelastic dynamics and strain compatibility. Phys. Rev. B **67**, 024114 (2003)
28. Balandraud, X., Zanzotto, G.: Stressed microstructures in thermally induced M9R-M18R martensites. J. Mech. Phys. Solids **55**, 194–224 (2007)
29. Pérez-Reche, F.J. et al.: Athermal character of structural phase transitions. Phys. Rev. Lett. **87**, 195701 (2001)
30. Truskinovsky, L., Vainchtein, A.: About the origin of the nucleation peak in transformational plasticity. J. Mech. Phys. Solids **52**, 1421–1446 (2004)
31. Kartha, S., Sethna, J.P.: Disorder-driven pretransitional tweed pattern in martensitic transformations. Phys. Rev. B **52**, 803–822 (1995)
32. Shenoy, S.R. et al.: Martensitic textures: Multiscale consequences of elastic compatibility. Phys. Rev. B **60**, R12537 (1999)
33. Ren, X., Truskinovsky, L.: Finite scale microstructures in 1-D elasticity. J. Elast. **59**, 319–355 (2000)
34. Dickman, R. et al.: Paths to Self-Organized Criticality. Braz. J. Phys. **30**, 27–41 (2000)
35. Cui, J. et al.: Combinatorial search of thermoelastic shape-memory alloys with extremely small hysteresis width. Nat. Mater. **5**, 286–290 (2006)
36. Pérez-Reche, F.J., Truskinovsky, L., Zanzotto, G.: Driving-induced crossover: From classical criticality to self-organized criticality. Phys. Rev. Lett. **101**, 230601 (2008)